

## Article

# Production of Al–Mn/WC Composite Coatings with Electrodeposition in AlCl<sub>3</sub>–NaCl–KCl–MnCl<sub>2</sub> Molten Salts

Wenjuan Qi <sup>1</sup>, Desheng Ding <sup>1</sup>, Weijie Luo <sup>1</sup>, Weiliang Jin <sup>2</sup>, Qian Kou <sup>1</sup>, Chuntao Ge <sup>1</sup> and Saijun Xiao <sup>1,\*</sup><sup>1</sup> School of Metallurgy Engineering, Anhui University of Technology, Ma'anshan 243032, China<sup>2</sup> Department of Metallurgy, Graduate School of Engineering, Tohoku University, Sendai 980-8579, Japan

\* Correspondence: xiaosaijunzj@yahoo.com

**Abstract:** The hardness and wear resistance of amorphous Al–Mn alloy coatings can be improved by incorporating ceramic particles into them to extend their application. In this paper, Al–Mn/WC composite coatings have been prepared with electrodeposition in stirred AlCl<sub>3</sub>–NaCl–KCl–MnCl<sub>2</sub> molten salts at 180 °C with the addition of WC particles. The effects of stirring speed (400–700 rpm) and cathode current density (15–75 mA/cm<sup>2</sup>) on the produced Al–Mn/WC composite coatings have been studied. At 600 rpm and 700 rpm, the Al–Mn/WC composite coatings exhibited the best uniform distribution of the embedded WC particles, with the tested microhardness value up to 650 HV<sub>0.1</sub>, compared with 530 HV<sub>0.1</sub> of the Al–Mn alloy. Moreover, under various cathode current densities, the best quality of the Al–Mn/WC composite coating was obtained at 55 mA/cm<sup>2</sup>, with a homogeneous distribution of WC particles and the highest microhardness value (670 HV<sub>0.1</sub>). It is expected that this method could be extended to be applied for the preparation of aluminum-based and magnesium-based ceramic composite coatings.

**Keywords:** AlCl<sub>3</sub>–NaCl–KCl–MnCl<sub>2</sub> molten salts; electrodeposition; WC particles; Al–Mn/WC composite coating



**Citation:** Qi, W.; Ding, D.; Luo, W.; Jin, W.; Kou, Q.; Ge, C.; Xiao, S. Production of Al–Mn/WC Composite Coatings with Electrodeposition in AlCl<sub>3</sub>–NaCl–KCl–MnCl<sub>2</sub> Molten Salts. *Coatings* **2023**, *13*, 1246. <https://doi.org/10.3390/coatings13071246>

Academic Editor: Stefan Lucian Toma

Received: 16 June 2023

Revised: 1 July 2023

Accepted: 5 July 2023

Published: 14 July 2023



**Copyright:** © 2023 by the authors. Licensee MDPI, Basel, Switzerland. This article is an open access article distributed under the terms and conditions of the Creative Commons Attribution (CC BY) license (<https://creativecommons.org/licenses/by/4.0/>).

## 1. Introduction

Amorphous Al–Mn alloy coatings have attracted considerable interest due to their promising chemical, physical, mechanical and corrosion-resistant properties [1–3], and they have been utilized to protect metals such as steels [4], magnesium alloys [5] and NdFeB magnets [6] against corrosion.

By improving the hardness and wear resistance of Al–Mn alloys, their applications can be broadened [7,8]. Numerous studies have demonstrated that Al-based composite coatings containing ceramic particles have increased hardness and improved wear resistance, and are capable of protecting metal substrates under harsh environments [9–11]. Currently, incorporated particles such as diamonds [12], SiO<sub>2</sub> [13], Al<sub>2</sub>O<sub>3</sub> [14], SiC [15], WC [16], TiB<sub>2</sub> [17] and CNT (carbon nanotubes) [18] are being used to prepare composite coatings. Therefore, it is worthwhile to explore the possibility of incorporating ceramic particles into amorphous Al–Mn alloy coatings in order to improve their quality.

Amorphous Al–Mn alloy coatings can be prepared using both molten salt electrodeposition [19–22] and room-temperature ionic solution electrodeposition [23–25]. Since room-temperature ionic solutions are highly volatile, expensive [24], mostly toxic and poorly biodegradable, and the synthesis of ionic liquids includes several steps involving highly toxic reagents [26], it is more advantageous to prepare Al–Mn alloys with electrodeposition in low-temperature inorganic molten salts. As an example, M. Jafarian et al. electrodeposited Al, Mn and Al–Mn alloys on aluminum electrodes in AlCl<sub>3</sub>–NaCl–KCl molten salts [20]. Ting-ting Cai [27] obtained good quality Al–Mn coatings with electrodeposition in an AlCl<sub>3</sub>–NaCl–KCl–MnCl<sub>2</sub> (0.5–2.0 wt.%) melt at 200–220 °C under cathode current densities of 26.7–48.0 mA/cm<sup>2</sup>.

Our group has produced Al/TiC nanocomposite coatings with electrodeposition in  $\text{AlCl}_3\text{-NaCl-KCl}$  molten salts with the addition of TiC nanoparticles [28]. TiC nanoparticles have been successfully incorporated into Al coatings with a uniform distribution, and the hardness of Al/TiC composite coatings was significantly improved compared with pure Al coatings; thus, this method can be extended to prepare Al-Mn-based composite coatings. Therefore, this paper focuses on investigating the possibility of electrodeposition in  $\text{AlCl}_3\text{-NaCl-KCl-MnCl}_2$  molten salts at 180 °C with the introduction of WC particles to prepare Al-Mn-based composite coatings incorporated with WC particles under a stirring state. Moreover, the effects of stirring speed and cathode current density on the incorporation of WC particles into Al-Mn coatings and their mechanical properties have been investigated.

## 2. Experimental

### 2.1. Preparation of NaCl-KCl Solid Salts Containing WC Particles

The procedure for preparing NaCl-KCl solid salts containing WC particles is illustrated in Figure 1. Using a planetary ball mill (HLXPM- $\phi 10 \times 4$ , Hengle, Wuhan, China), NaCl (99%, Sinopharm, Shanghai, China) and KCl (99%, Sinopharm) were pre-dried in an oven for 48 h at 200 °C, mixed in a mole ratio of 1:1, and then ball milled in a 316 stainless steel grinding jar for 2 h. WC particles (average size, 400 nm, Aladdin Biochemical Technology Co., Ltd., Shanghai, China) were blended with ball-milled NaCl-KCl salts at a mass ratio of 1:1, ultrasonically dispersed in acetone for 2 h (100 kHz), and finally dried at 120 °C for 1 h in a vacuum drying oven to obtain NaCl-KCl solid salts containing WC particles.

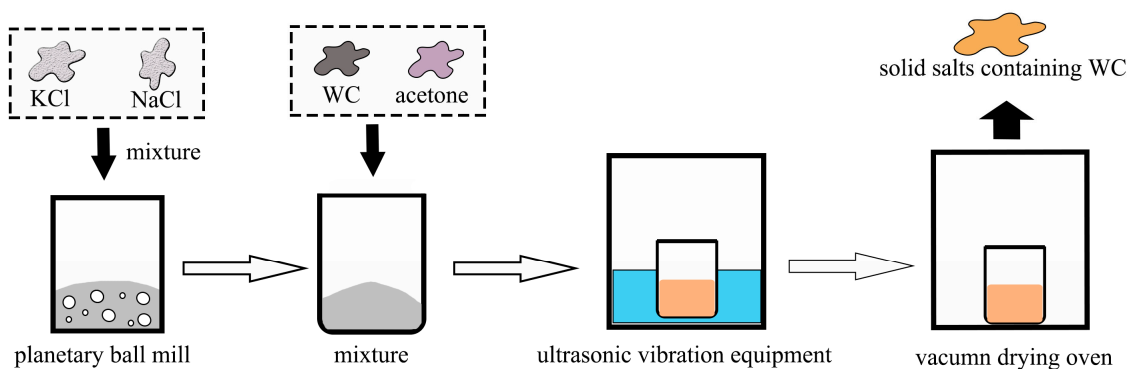


**Figure 1.** Schematic diagram of the preparation process of NaCl-KCl solid salts containing WC particles.

### 2.2. Electrodeposition Process for Producing Al-Mn/WC Composite Coatings

An  $\text{AlCl}_3\text{-NaCl-KCl}$  mixture with a molar ratio of 66:17:17 was selected as the electrolyte.  $\text{AlCl}_3$  (99%, Aladdin Biochemical Technology Co., Ltd.) was weighed and ground in a glove box protected by an argon atmosphere and mixed with KCl and NaCl in the glove box. Then, 1.5 wt.%  $\text{MnCl}_2$  (>99%, Aladdin Biochemical Technology Co., Ltd.) was added to obtain  $\text{AlCl}_3\text{-NaCl-KCl-MnCl}_2$  salts.  $\text{MnCl}_2$  was dried in a vacuum oven at 200 °C for 10 h before use.

As shown in Figure 2, an  $\text{AlCl}_3\text{-NaCl-KCl-MnCl}_2$  mixture was placed in a quartz crucible under an argon atmosphere, which was heated to 180 °C in an oil bath. After it was melted, NaCl-KCl solid salts containing WC particles were added to the molten salts through the filling hole and stirred using a mechanical stirring paddle to form  $\text{AlCl}_3\text{-NaCl-KCl-MnCl}_2$  molten salts in which the WC particles can be well suspended. A 25 mm  $\times$  5 mm  $\times$  0.5 mm sheet of 304 stainless steel was used as the cathode and a 25 mm  $\times$  5 mm  $\times$  3 mm sheet with high purity (99.999 wt.%) aluminum was used as the anode. The cathode and anode were positioned symmetrically and parallel to each other, with the stirring paddle placed in the center. After electrodeposition, the cathodes were removed, cleaned in deionized water, dried, and characterized.

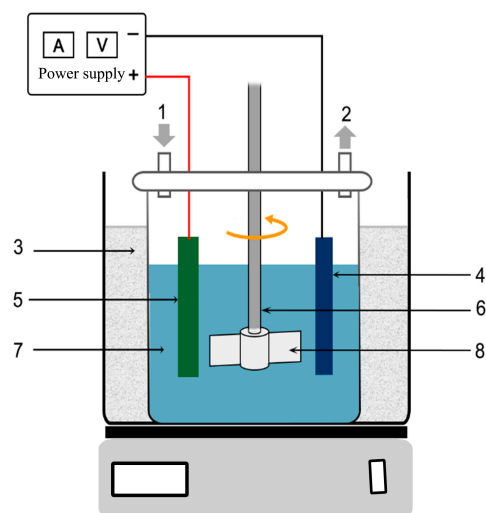


**Figure 2.** Schematic diagram of the molten salt electrodeposition device under mechanical stirring. 1. Argon gas inlet; 2. outlet; 3. silicone oil; 4. stainless steel cathode; 5. aluminum anode; 6. rotating rod; 7. molten salts electrolyte; 8. stirring paddle.

The effect of different stirring speeds (400 rpm, 500 rpm, 600 rpm and 700 rpm) on the electrodeposition of Al–Mn/WC composite coatings was studied in  $\text{AlCl}_3\text{–NaCl–KCl–MnCl}_2$  molten salts under a current density of  $55 \text{ mA/cm}^2$  with a WC particle concentration of  $20 \text{ g/L}$  at  $180^\circ\text{C}$ .

In addition, the influence of different cathode current densities ( $15 \text{ mA/cm}^2$ ,  $35 \text{ mA/cm}^2$ ,  $55 \text{ mA/cm}^2$  and  $75 \text{ mA/cm}^2$ ) on the produced Al–Mn/WC composite coatings was investigated in the same molten salts under a rotating speed of 700 rpm with a WC particle concentration of  $30 \text{ g/L}$  at  $180^\circ\text{C}$ . In order to pass the same charge at different current densities, the electrodeposition time was 37 min, 16 min, 10 min and 7.5 min, respectively.

### 2.3. Characterization of WC Raw Materials and Coatings

The WC raw material and the surface and cross-sectional morphologies of the composite coatings were examined using scanning electron microscopy (SEM) (Regulus 8220, HITACHI and JSM-6510, JEOL, Tokyo, Japan). X-ray diffraction (XRD, Tokyo, Japan) (Smart Lab, Rigaku, voltage: 40 kV, current: 40 mA, scan rate:  $10^\circ/\text{min}$ ) was used to analyze their phase composition. A Vickers microhardness tester (Q30A+, Qness, Salzburg, Austria) was employed to measure the Vickers hardness using a load of 0.98 N with a dwell time of 10 s. Six indentation tests on various parts of each coating were conducted to ensure reliability.

## 3. Results and Discussion

### 3.1. Preparation of Al–Mn/WC Composite Coatings at Various Rotating Speeds

The as-received WC particles were characterized by XRD and SEM, with the results shown in Figure 3. From the XRD analysis results in Figure 3a, it is obvious that the WC particles were pure. In addition, from Figure 3b, it can be found that the WC particles had a particle size smaller than 500 nm, with a relatively uniform particle size distribution.

Electrodeposition was carried out in  $\text{AlCl}_3\text{–NaCl–KCl–MnCl}_2$  molten salts with the addition of WC particles ( $20 \text{ g/L}$ ) at  $180^\circ\text{C}$  under a cathode current density of  $55 \text{ mA/cm}^2$ . The rotating rate of the mechanical stirring paddle ranged from 400 rpm to 700 rpm. A photograph depicting the typical appearance of the produced coating (under a rotating rate of 500 rpm) is shown in Figure 4a, exhibiting a relatively flat and metallic appearance. Figure 4b presents the XRD results of the obtained composite coatings at various stirring rates. For the XRD result corresponding to no addition of WC particles, there existed an amorphous hump with  $2\theta$  in the range of  $40\text{--}48^\circ$ , which corresponded to amorphous Al–Mn [27]. Moreover, diffraction peaks for 304 stainless steel substrates and Al can also be detected. After the introduction of WC particles, diffraction peaks of WC can be detected,

indicating successful incorporation of WC particles into the Al–Mn alloy at a stirring rate from 400 rpm to 700 rpm in the  $\text{AlCl}_3\text{--NaCl--KCl--MnCl}_2$  melt at 180 °C.

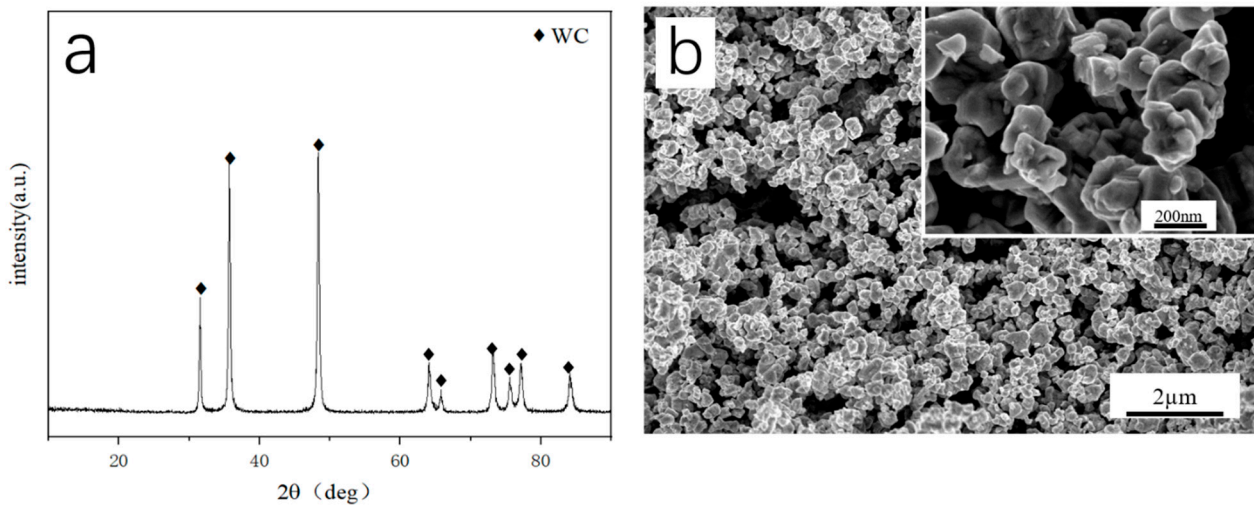


**Figure 3.** XRD (a) and SEM (b) images of the as-received WC particles.

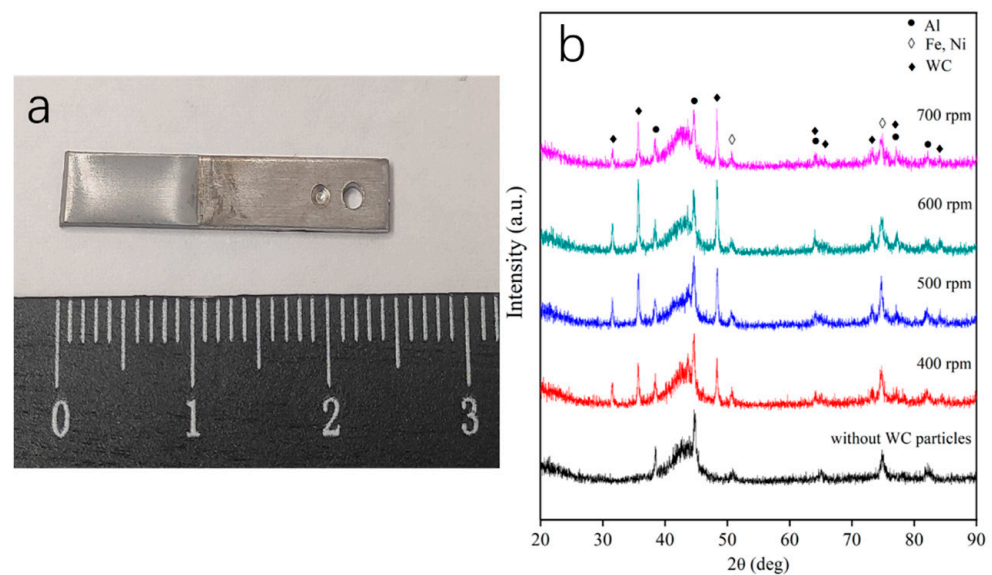


**Figure 4.** (a) Typical appearance (500 rpm) and (b) XRD patterns (400–700 rpm) of Al–Mn/WC composite coatings with electrodeposition under a cathode current density of 55  $\text{mA}/\text{cm}^2$  in the  $\text{AlCl}_3\text{--NaCl--KCl--MnCl}_2$  melt at 180 °C (WC particle concentration, 20 g/L).

Subsequently, the surface morphologies of Al–Mn/WC composite coatings prepared at different stirring speeds were analyzed with SEM (backscattered electron mode) as shown in Figure 5, in which the bright white areas corresponded to the WC particles embedded in the coatings. At a rotating rate of 400 rpm (Figure 5a), it can be seen that the incorporated WC particles tended to aggregate. When it was increased to 500 rpm, the agglomeration of WC particles decreased, and an increased amount of WC particles was embedded. With the increase in the stirring rate to 600 and 700 rpm, a better distribution of WC particles was demonstrated.

The cross-sectional SEM images of the Al–Mn/WC composite coatings prepared at different rotating speeds are presented in Figure 6. It can be seen that the Al–Mn/WC coatings were dense and well bonded to the substrate. The change in the stirring rate had an insignificant effect on the thickness of the composite coatings. At 400 rpm, there existed severe aggregation of WC particles, especially on the surface, corresponding to the result in

Figure 5a, resulting in a slightly reduced thickness. An uneven distribution of WC particles was also observed. At 500 rpm, the distribution of WC particles became more uniform. The further increase in the stirring rate to 600 rpm and 700 rpm resulted in reduced aggregation of WC particles and more even distribution of them in the coatings, which is in agreement with the SEM analysis results of the Al–Mn/WC surface as shown in Figure 5c,d.

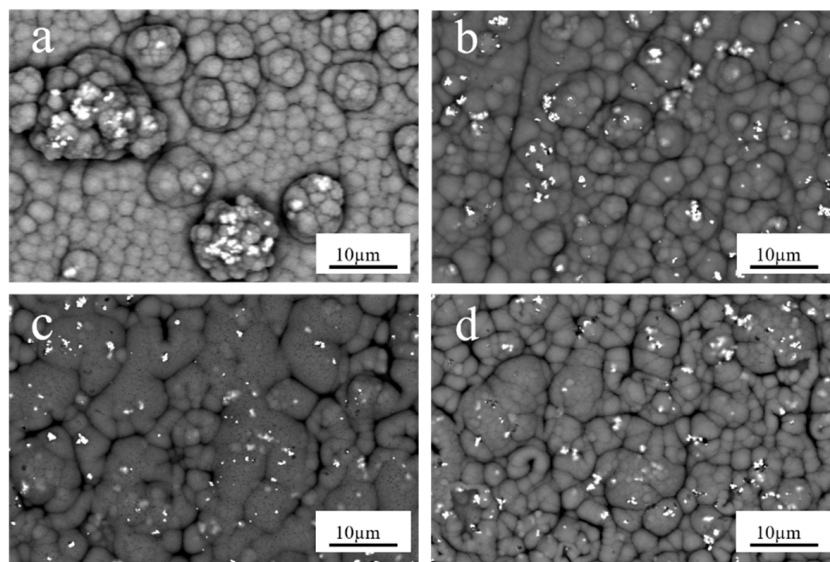


**Figure 5.** SEM images of the surface of the obtained Al–Mn/WC composite coatings with electrodeposition under a cathode current density of  $55 \text{ mA/cm}^2$  in the  $\text{AlCl}_3\text{--NaCl--KCl--MnCl}_2$  melt at  $180^\circ\text{C}$  (WC particle concentration,  $20 \text{ g/L}$ ) ((a) 400 rpm; (b) 500 rpm; (c) 600 rpm; (d) 700 rpm).

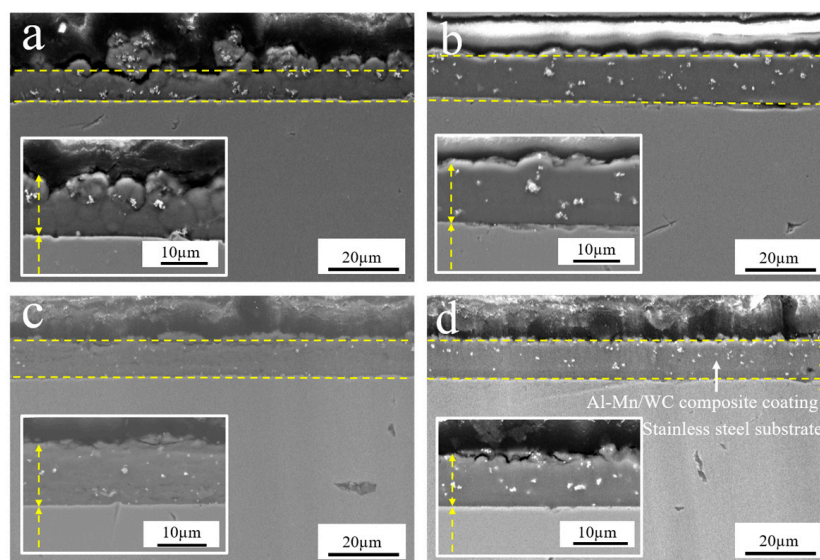


**Figure 6.** SEM images of the cross-sections of the obtained Al–Mn/WC composite coatings with electrodeposition under a cathode current density of  $55 \text{ mA/cm}^2$  in the  $\text{AlCl}_3\text{--NaCl--KCl--MnCl}_2$  melt at  $180^\circ\text{C}$  (WC particle concentration,  $20 \text{ g/L}$ ) ((a) 400 rpm; (b) 500 rpm; (c) 600 rpm; (d) 700 rpm).

Furthermore, the microhardness of these samples was tested to evaluate the effect of incorporating WC particles into the Al–Mn alloy. At the same time, it was noticed that the Mn content in the Al–Mn/WC composite coatings produced at different speeds fluctuated within the range of 28–32 wt.%. To avoid the effect of Mn content change on the values of hardness, the hardness of Al–Mn coatings with different Mn content was measured and analyzed, with the results presented in Figure 7a. As the Mn content increased, the

hardness of the Al–Mn coating increased gradually. However, at a Mn content of 27 wt.%, the hardness growth rate became slower, which was in agreement with the results reported by Uchida [29]. In Figure 7a, it can be seen that the hardness did not vary significantly with the Mn content in the range of 28 wt.% to 32 wt.%, ranging from 510 HV<sub>0.1</sub> to 530 HV<sub>0.1</sub>.

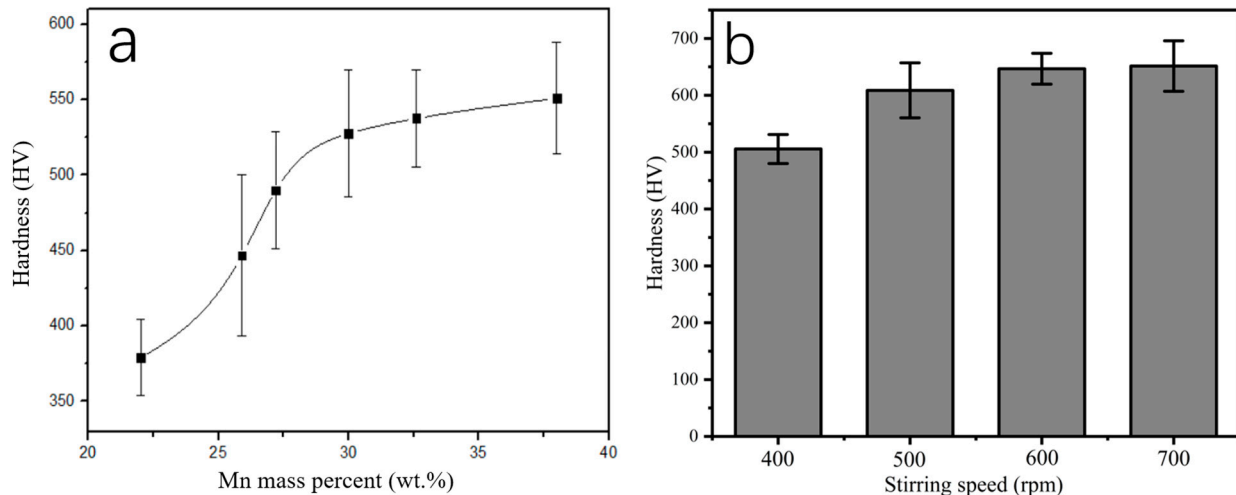


**Figure 7.** (a) Microhardness of the Al–Mn coating at different Mn contents; (b) Microhardness of the Al–Mn/WC composite coating at different stirring speeds.

At various stirring speeds, Figure 7b presents the microhardness of Al–Mn/WC composite coatings. The hardness of the Al–Mn/WC composite coatings increased with the increase in stirring speed. With a rotating speed of 600 rpm and 700 rpm, the value of the microhardness could reach 650 HV<sub>0.1</sub>. It was also higher than 530 HV<sub>0.1</sub> for the Al–Mn coating. As a result, the variation in hardness of Al–Mn/WC composite coatings prepared at different rotating speeds is mainly due to the enhanced inclusion of WC particles in the coating with a more uniform distribution.

During the electrodeposition, as the stirring speed increases, the frequency of collision between WC particles and the electrode surface increases, leading to increased chances for WC particles to be captured by electrodeposited Al–Mn. On the other hand, employment of stirring speeds that are too high increase the impact of molten salt fluid on the electrode surface, which allows WC particles that have been captured by the electrode surface to detach from it and reenter into the molten salts [30,31]. In the present study, at a low stirring rate, the gravitational effect of WC particles dominates due to their high density (15.77 g/cm<sup>3</sup>). Thus, they do not suspend well in the molten salts, resulting in a relatively small amount of WC incorporated in the Al–Mn coating. As the stirring rate increases, the WC particles overcome these gravitational effects, resulting in better suspension and an increase in WC amount in the Al–Mn coating. When the speed is further raised to 700 rpm, although the frequency of collisions between WC particles and the electrode increases, the large impact of the molten salt fluid probably causes WC particles that are captured on the electrode surface to divorce from it again. As a result, at 600 rpm and 700 rpm, the incorporation results are similar, demonstrating a good distribution of WC particles and the highest coating hardness. Simultaneously, the incorporation of WC particles in the Al–Mn coating leads to an improved value of hardness, compared with that of the Al–Mn coating.

### 3.2. Preparation of Al–Mn/WC Composite Coatings at Various Current Densities

Electrodeposition was conducted with a WC particles concentration of 30 g/L at cathode current densities of 15–75 mA/cm<sup>2</sup>. In this case, a stirring rate of 700 rpm was selected according to the experimental results in Section 3.1. The XRD pattern results of the obtained composite coatings are shown in Figure 8 (not including the result for the composite coating at 15 mA/cm<sup>2</sup> because of its poor quality). It can be observed that

there existed an amorphous region between 40 and 48°, corresponding to the formation of Al–Mn, and diffraction peaks of WC, stainless steel substrates and Al, demonstrating successful incorporation of WC particles into the Al–Mn alloy at current densities from 35 to 75 mA/cm<sup>2</sup> in the AlCl<sub>3</sub>–NaCl–KCl–MnCl<sub>2</sub> melt at 180 °C.

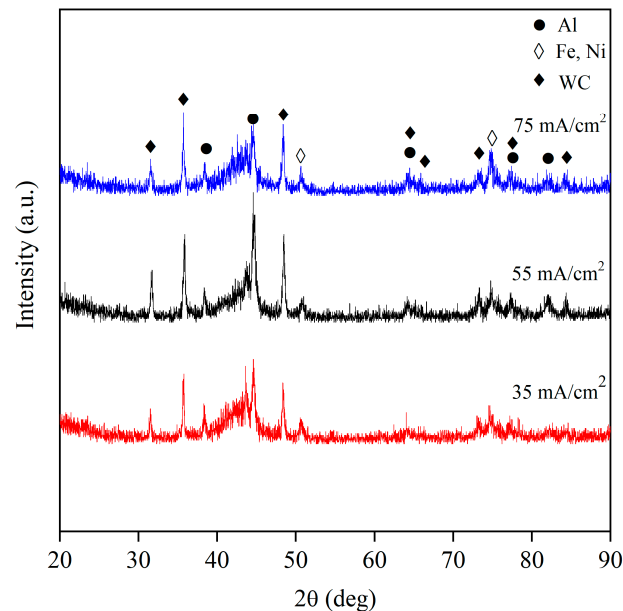


**Figure 8.** XRD patterns of Al–Mn/WC composite coatings with electrodeposition under cathode current densities of 35–75 mA/cm<sup>2</sup> with a stirring rate of 700 rpm in the AlCl<sub>3</sub>–NaCl–KCl–MnCl<sub>2</sub> melt at 180 °C (WC particle concentration, 30 g/L).

The surface morphologies of Al–Mn/WC composite coatings prepared with electrodeposition at varying current densities are shown in Figure 9. Locations with bright white particles corresponded to WC particles. As shown in Figure 9, the content of WC particles in the Al–Mn/WC composite coating increased with elevated current density, and the WC particles were dispersed most uniformly at the current density of 55 mA/cm<sup>2</sup>.

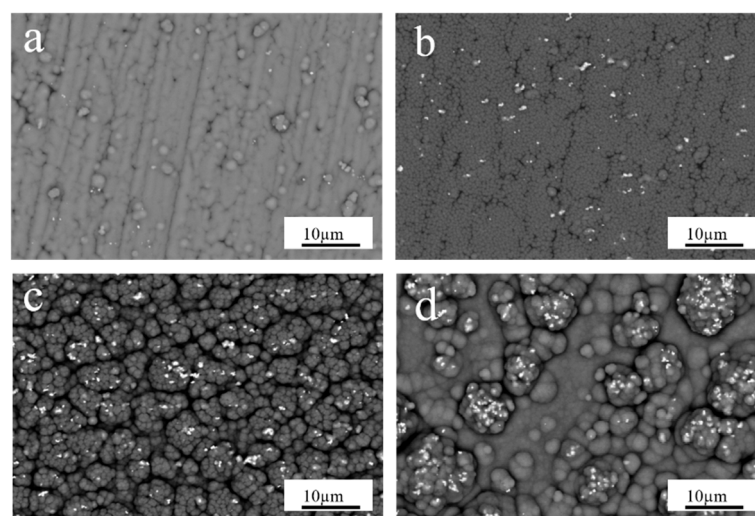


**Figure 9.** SEM images of the surface of the obtained Al–Mn/WC composite coatings using electrodeposition with a stirring rate of 700 rpm in the AlCl<sub>3</sub>–NaCl–KCl–MnCl<sub>2</sub> melt at 180 °C (WC particle concentration, 30 g/L) ((a) 15 mA/cm<sup>2</sup>; (b) 35 mA/cm<sup>2</sup>; (c) 55 mA/cm<sup>2</sup>; (d) 75 mA/cm<sup>2</sup>).

SEM analysis of the cross-sections of Al–Mn/WC composite coatings prepared with electrodeposition at various current densities was conducted, and the obtained results

are shown in Figure 10. It can be observed that the thickness of the Al–Mn/WC coating prepared under a current density of 15 mA/cm<sup>2</sup> was smaller than those under other conditions, based on the same passed charge under different cathode current densities. This coating contained a small amount of incorporated WC particles, with poor adhesion. Increasing the current density to 30 mA/cm<sup>2</sup> and 55 mA/cm<sup>2</sup> resulted in enhanced thickness of the coating as well as the content of WC particles. These coatings, with good adhesion, coherence and high compactness, included uniform distributions of WC particles. As the current density increased to 75 mA/cm<sup>2</sup>, the flatness of the coating was reduced, with a degraded distribution of WC particles and their amount was decreased slightly.

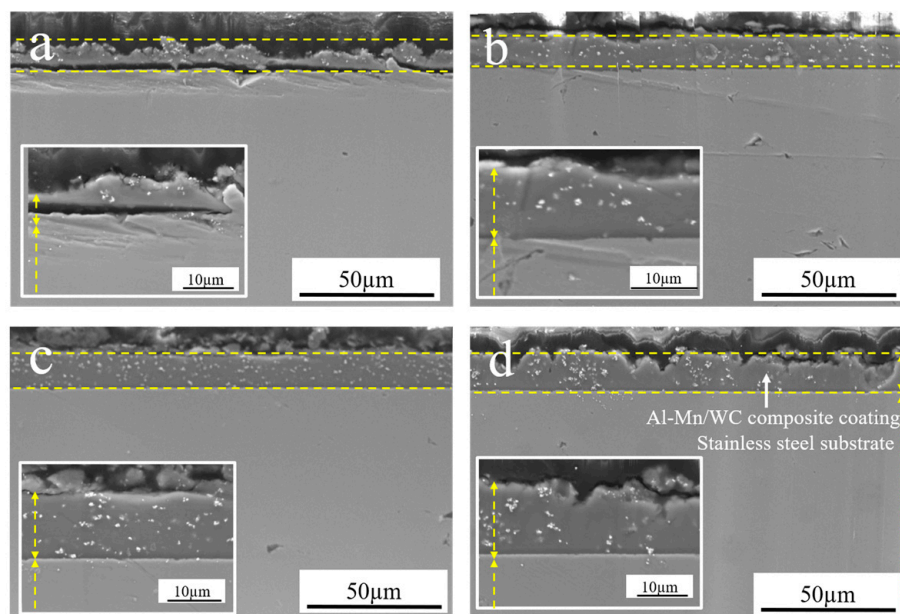


**Figure 10.** SEM images of the cross-sections of the obtained Al–Mn/WC composite coatings using electrodeposition with a stirring rate of 700 rpm in the AlCl<sub>3</sub>–NaCl–KCl–MnCl<sub>2</sub> melt at 180 °C (WC particle concentration, 30 g/L) ((a) 15 mA/cm<sup>2</sup>; (b) 35 mA/cm<sup>2</sup>; (c) 55 mA/cm<sup>2</sup>; (d) 75 mA/cm<sup>2</sup>).

Under different current density conditions, the Mn content of Al–Mn/WC composite coatings ranged from 29 wt.% to 32 wt.%. According to Figure 7a, the hardness of Al–Mn coatings within this Mn content range was between 520 HV<sub>0.1</sub> and 530 HV<sub>0.1</sub>, which indicated that Mn content variation had no significant effect on coating hardness in this range. As shown in Figure 11, the hardness value of composite coatings obtained at 35–75 mA/cm<sup>2</sup> was tested and analyzed, among which the hardness of the Al–Mn/WC coating at 55 mA/cm<sup>2</sup> was the highest, reaching 670 HV<sub>0.1</sub>. At 75 mA/cm<sup>2</sup>, the hardness value was lower than that of the coating at 55 mA/cm<sup>2</sup>, with a wider error bar, exhibiting larger instability. These results were in agreement with SEM analysis results shown in Figure 10.

The cathode current density has a large effect on the quality and the incorporation of particles for the coating. The growth rate of the coating controlled by the cathode current density should match the transporting rate of particles towards the electrode dominated by the stirring rate, in order to form a coating with a uniform distribution of particles in it. As can be seen from Figures 9 and 10, at the 15 mA/cm<sup>2</sup> current density, most WC particles delivered to the cathode surface are probably returned to the molten salts by the stirring fluid before they are completely embedded into the Al–Mn coating, due to its relatively slow growth rate, so the Al–Mn/WC composite coating contains a small amount of WC particles. Furthermore, these detached WC particles also remove some of the deposited Al–Mn metal, reducing the current efficiency and making the Al–Mn/WC composite coating thin. In addition, such low current density leads to electrodeposition

a coating with poor quality. By increasing the current density, the WC particles on the cathode surface are easy to be embedded and covered by the relatively quick deposition of the Al–Mn metal, improving particle incorporation efficiency and current efficiency [32]. However, with a further increase in the current density to  $75 \text{ mA/cm}^2$ , the Al–Mn alloy is deposited extremely quickly, while perhaps the transporting rate of WC particles using mechanical stirring could not catch up with the deposition speed of Al–Mn [33]. In this case, the amount of embedded WC particles is slightly reduced. Moreover, a high current density tends to cause concentration polarization [34], forming dendrites and uneven coating surfaces for the deposited Al–Mn/WC coating, as illustrated in Figure 10d. Therefore, the quality of the Al–Mn/WC composite coating at  $55 \text{ mA/cm}^2$  is the best, and the dispersion of the WC particles is the most homogeneous, demonstrating the highest microhardness.

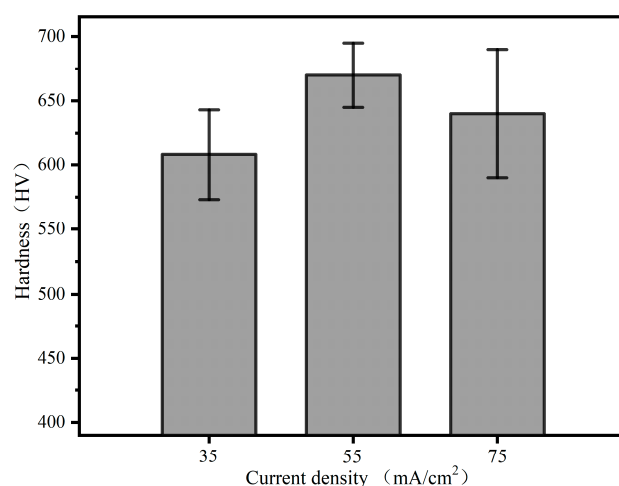


**Figure 11.** Microhardness of Al–Mn/WC composite coatings obtained at different cathode current densities.

#### 4. Conclusions

We have conducted investigations on electrodepositing Al–Mn/WC composite coatings in an  $\text{AlCl}_3$ – $\text{NaCl}$ – $\text{KCl}$ – $\text{MnCl}_2$  melt at  $180^\circ\text{C}$  with the introduction of WC particles under a stirring state. The conclusions are as follows.

- (1) With the assistance of mechanical stirring, Al–Mn/WC composite coatings can be prepared using electrodeposition with an enhanced value of microhardness compared with Al–Mn alloy coatings.
- (2) At different rotating speeds between 400 rpm and 700 rpm, a better distribution of incorporated WC particles caused by the increased rotating speeds was found, due to the better suspension of WC particles. At 600 rpm and 700 rpm, the highest microhardness value of the Al–Mn/WC composite coatings was reached at  $650 \text{ HV}_{0.1}$ , compared with  $530 \text{ HV}_{0.1}$  of Al–Mn coatings with a similar Mn content.
- (3) Under various cathode current densities ranging from  $15 \text{ mA/cm}^2$  to  $55 \text{ mA/cm}^2$ , the amount of embedded WC particles and their distribution in Al–Mn/WC composite coatings have been improved. A further increase to  $75 \text{ mA/cm}^2$  resulted in a slightly reduced amount of embedded WC particles and an uneven distribution of them. Therefore, the highest microhardness value ( $670 \text{ HV}_{0.1}$ ) was obtained at  $55 \text{ mA/cm}^2$ .

**Author Contributions:** Conceptualization, W.Q. and S.X.; Methodology, W.Q., D.D., W.J., Q.K., C.G. and S.X.; Validation, W.Q.; Formal analysis, W.L. and W.J.; Resources, D.D., Q.K. and C.G.; Data curation, W.Q.; Writing—original draft, W.Q.; Writing—review & editing, S.X.; Supervision, S.X. All authors have read and agreed to the published version of the manuscript.

**Funding:** This research was financially supported by the Innovation and Entrepreneurship Training Programme for college students in the Anhui Province (S202110360154).

**Institutional Review Board Statement:** Not applicable.

**Informed Consent Statement:** Not applicable.

**Data Availability Statement:** Not applicable.

**Acknowledgments:** This research was financially supported by the Innovation and Entrepreneurship Training Programme for college students in the Anhui Province (S202110360154).

**Conflicts of Interest:** The authors declare no conflict of interest.

## References

1. Peng, D.; Cong, D.; Song, K.; Ding, X.; Wang, X.; Bai, Y.; Yang, X.; Yin, C.; Zhang, Y.; Rao, J.; et al. Mirror-like Bright Al-Mn Coatings Electrodeposition from 1-Ethyl-3 Methylimidazolium Chloride-AlCl<sub>3</sub>-MnCl<sub>2</sub> Ionic Liquids with Pyridine Derivatives. *Materials* **2021**, *14*, 6226. [[CrossRef](#)] [[PubMed](#)]
2. Reffass, M.; Berziou, C.; Rebere, C.; Billard, A.; Creus, J. Corrosion behaviour of magnetron-sputtered Al<sub>1-x</sub>Mn<sub>x</sub> coatings in neutral saline solution. *Corros. Sci.* **2010**, *52*, 3615–3623. [[CrossRef](#)]
3. Mraied, H.; Cai, W.; Sagüés, A.A. Corrosion resistance of Al and Al-Mn thin films. *Thin Solid Films* **2016**, *615*, 391–401. [[CrossRef](#)]
4. Dobruchowska, E.; Gilewicz, A.; Warcholinski, B.; Libralesso, L.; Batory, D.; Szparaga, L.; Murzynski, D.; Ratajski, J. Al-Mn based coatings deposited by cathodic arc evaporation for corrosion protection of AISI 4140 alloy steel. *Surf. Coat. Technol.* **2019**, *362*, 345–354. [[CrossRef](#)]
5. Zhang, J.; Yan, C.; Wang, F. Electrodeposition of Al-Mn alloy on AZ31B magnesium alloy in molten salts. *Appl. Surf. Sci.* **2009**, *255*, 4926–4932. [[CrossRef](#)]
6. Ding, J.; Xu, B.; Ling, G. Al-Mn coating electrodeposited from ionic liquid on NdFeB magnet with high hardness and corrosion resistance. *Appl. Surf. Sci.* **2014**, *305*, 309–313. [[CrossRef](#)]
7. Schaedler, T.A.; Chan, L.J.; Clough, E.C.; Stilke, M.A.; Hundley, J.M.; Masur, L.J. Nanocrystalline Aluminum Truss Cores for Lightweight Sandwich Structures. *JOM* **2017**, *69*, 2626–2634. [[CrossRef](#)]
8. Hilty, R.D.; Masur, L.J. On the Formation of Lightweight Nanocrystalline Aluminum Alloys by Electrodeposition. *JOM* **2017**, *69*, 2621–2625. [[CrossRef](#)]
9. Walsh, F.C.; Wang, S.; Zhou, N. The Electrodeposition of Composite Coatings: Diversity, Applications and Challenges. *Curr. Opin. Electrochem.* **2020**, *20*, 8–19. [[CrossRef](#)]
10. Sankara Narayanan, T.S.N.; Seshadri, S.K. *Electro- and Electroless Deposited Composite Coatings: Preparation, Characteristics, and Applications*; American Cancer Society: Philadelphia, PA, USA, 2012; Volume 20.
11. Low, C.T.J.; Wills, R.G.A.; Walsh, F. Electrodeposition of composite coatings containing nanoparticles in a metal deposit. *Surf. Coat. Technol.* **2006**, *201*, 371–383. [[CrossRef](#)]
12. Fu, Y.Y.; Chen, X.Y.; Zhang, B.T.; Gong, Y.; Zhang, H.; Li, H. Fabrication of nanodiamond reinforced aluminum composite coatings by flame spraying for marine applications. *Mater. Today Commun.* **2018**, *17*, 46–52. [[CrossRef](#)]
13. Fang, L.; Xu, Y.; Gao, L.; Suo, X.; Gong, J.; Li, H. Cold-Sprayed Aluminum-Silica Composite Coatings Enhance Anti-wear/Anticorrosion Performances of AZ31 Magnesium Alloy. *Adv. Mater. Sci. Eng.* **2018**, *2018*, 3215340. [[CrossRef](#)]
14. Yang, W.M.; Li, X.Y.; Du, D.X.; Cao, Y.; Leng, Y. Structure of Al-based composite coatings prepared by thermal diffusion of the arc-ion plating Al coatings. *Int. J. Mod. Phys. B* **2019**, *33*, 1940021. [[CrossRef](#)]
15. Wang, P.; Gao, Z.; Li, J.Z.; Cheng, D.; Niu, J. Research on reaction brazing of Ti layer-coated SiCp/Al composites using Al-based filler metal foil. *Compos. Interfaces* **2019**, *26*, 1057–1068. [[CrossRef](#)]
16. Li, C.G.; Li, S.; Liu, C.M.; Zhang, Y.; Deng, P.; Guo, Y.; Wang, J.; Wang, Y. Effect of WC addition on microstructure and tribological properties of bimodal aluminum composite coatings fabricated by laser surface alloying. *Mater. Chem. Phys.* **2019**, *234*, 9–15. [[CrossRef](#)]
17. Yang, F.; Qin, Q.; Shi, T.; Chen, C.; Guo, Z. Surface strengthening aluminum alloy by in-situ TiC-TiB<sub>2</sub> composite coating. *Ceram. Int.* **2019**, *45*, 4243–4252. [[CrossRef](#)]
18. Khasanova, R.S.; Komarov, S.V.; Zadorozhnyy, V.Y. Mechanical plating of Al/CNT composite coatings on aluminum substrates. *J. Alloys Compd.* **2017**, *707*, 238–244. [[CrossRef](#)]
19. Li, J.C.; Nan, S.H.; Jiang, Q. Study of the electrodeposition of Al-Mn amorphous alloys from molten salts. *Surf. Coat. Technol.* **1998**, *106*, 135–139. [[CrossRef](#)]
20. Jafarian, M.; Maleki, A.; Danaee, I.; Gopal, F.; Mahjani, M.G. Electrodeposition of Al, Mn, and Al-Mn Alloy on aluminum electrodes from molten salt (AlCl<sub>3</sub>-NaCl-KCl). *J. Appl. Electrochem.* **2009**, *39*, 1297–1303. [[CrossRef](#)]
21. Stafford, G.R. Electrodeposition of an aluminum-manganese metallic glass from molten salts. *J. Electrochem. Soc.* **1989**, *136*, 635–639. [[CrossRef](#)]
22. Gu, Y.K.; Liu, J.; Qu, S.; Deng, Y.; Han, X.; Hu, W.; Zhong, C. Electrodeposition of alloys and compounds from high-temperature molten salts. *J. Alloys Compd.* **2017**, *690*, 228–238. [[CrossRef](#)]
23. Chen, J.; Xu, B.; Ling, G. Amorphous Al-Mn coating on NdFeB magnets: Electrodeposition from AlCl<sub>3</sub>-EMIC-MnCl<sub>2</sub> ionic liquid and its corrosion behavior. *Mater. Chem. Phys.* **2012**, *134*, 1067–1071. [[CrossRef](#)]

24. Ispas, A.; Vlaic, C.A.; Camargo, M.K.; Bund, A. Electrochemical Deposition of Aluminum and Aluminum-Manganese Alloys in Ionic Liquids. *ECS Trans.* **2016**, *75*, 15. [[CrossRef](#)]
25. Maniam, K.K.; Paul, S. A Review on the Electrodeposition of Aluminum and Aluminum Alloys in Ionic Liquids. *Coatings* **2021**, *11*, 80. [[CrossRef](#)]
26. Jesus, S.; Filho, R.M. Are ionic liquids eco-friendly? *Renew. Sustain. Energy Rev.* **2022**, *157*, 112039. [[CrossRef](#)]
27. Cai, T.T. Study of Al-Mn Alloy Plating on Steel Surface and Its Corrosion Resistance. Master's Thesis, Northeastern University, Shenyang, China, 2014.
28. Ding, D.S.; Jin, W.L.; Luo, W.J.; Ge, C.T.; Kou, Q.; Xiao, S.J.; Zhang, J. Preparation of Al/TiC Nanocomposite Coatings on 304 Stainless Steel via Electrodeposition in Inorganic Molten Salts. *Int. J. Electrochem. Sci.* **2021**, *16*, 21114. [[CrossRef](#)]
29. Uchida, J.; Shibuya, A.; Tsuda, T.; Yamamoto, Y.; Seto, H. Al-Mn electroplating by molten salt electrolysis. *J. Surf. Fish. Soc. Jpn.* **1991**, *42*, 201–205.
30. Zhan, C.W.; Ge, Y.L.; Tian, L.X.; Wang, S.X.; Yang, Y.K.; Lian, Z.P.; Du, L. Effect of stirring speed and particle size on the amount of Ni-CBN composite by composite electrodeposition and analysis of the mechanism. *Electroplat. Finish.* **2022**, *44*, 1–5.
31. Cui, P.F.; Zhang, K.Y.; Zhou, Z.Y.; Li, Y.G.; Yang, K.L. Effect of stirring rate on the corrosion resistance of electrodeposited Ni-Sn/TiO<sub>2</sub> composite coatings. *Steel Vanadium Titan.* **2020**, *41*, 40–44.
32. Zhang, Q.; Tan, J.; Xie, F.K.; Meng, L.D.; Zang, Y.; Zhu, X.Y. Effect of current density on the organization and properties of Co-Ni-Cr<sub>3</sub>C<sub>2</sub> composite plating by jet electrodeposition. *Surf. Technol.* **2020**, *49*, 191–199.
33. Sadowska-mazur, J.; Warwick, M.E. A preliminary study of the electrodeposition of tin and non-metallic particles. *Plat. Surf. Finish.* **1985**, *72*, 120–125.
34. Léo, F.; Vincent, B.; Vincent, F.; Henri, S.; Christophe, T. Equivalent Electrical Model for High Current Density Zinc Electrodeposition: Investigation through Polarization Curves and Electrochemical Impedance Spectroscopy. *Int. J. Electrochem. Sci.* **2023**, *18*, 100185.

**Disclaimer/Publisher's Note:** The statements, opinions and data contained in all publications are solely those of the individual author(s) and contributor(s) and not of MDPI and/or the editor(s). MDPI and/or the editor(s) disclaim responsibility for any injury to people or property resulting from any ideas, methods, instructions or products referred to in the content.